Journal of Theoretical and Applied Vibration and Acoustics 11 (1) 57-72 (2025)

I S A V

Journal of Theoretical and Applied Vibration and Acoustics

journal homepage: http://tava.isav.ir

Hybrid deep learning for nonlinear acoustic-driven flame dynamics and experimental validation

Mohammad Ali Akhtardanesh [a], **Ensieh Alipour** [a], **Mohammad Farshchi** [b,*]

[a] *Ph.D. Candidate, Aerospace Engineering Department, Sharif University of Technology, Tehran, IRAN.*

[b] *Full Professor, Aerospace Engineering Department, Sharif University of Technology, Tehran, IRAN.*

Research Article

ARTICLE INFO

Article history:
Received 7 October 2024

Received in revised form
20 January 2025

Accepted 6 March 2025

Available online 14 May 2025

Keywords:
Partially premixed flame

Acoustic wave

Convolutional neural network

Deep learning

Combustion instability

ABSTRACT

This study proposes a hybrid deep-learning model that combines Convolutional Neural Networks (CNNs) with a Transformer Encoder to investigate the nonlinear dynamics of a laminar, partially premixed counterflow flame under acoustic excitation. The model was trained on experimental data obtained from a combustion instability laboratory. OH* chemiluminescence was employed to measure flame responses across a frequency range of 20 to 350 Hz and pressure amplitudes extending up to the extinction threshold. The research explores the intricate interactions between acoustic waves and flame dynamics, providing insights into how varying amplitudes and frequencies influence heat release rates. Despite inherent limitations in the dataset, the model demonstrated a robust ability to accurately approximate the flame transfer function, successfully replicating chemiluminescence signals and forecasting flame reactions to diverse acoustic excitations. Additionally, the repeatability of the flame structure was rigorously validated through high-speed imaging and image processing techniques, confirming consistent flame characteristics over multiple testing cycles. The results underline the significant promise of the hybrid deep-learning approach as a reliable tool for predicting flame behavior in complex acoustic environments, offering practical implications for mitigating combustion instabilities in various engineering applications. This research represents a significant step forward in applying machine learning techniques to enhance the predictability and control of flame dynamics in real-world systems.

© 2025 Iranian Society of Acoustics and Vibration, All rights reserved.

* Corresponding author.
E-mail address(es): farshchi@sharif.edu (M. Farshchi)

http://dx.doi.org/10.22064/tava.2025.2042805.1254

1. Introduction

Large-amplitude pressure variations resulting from thermoacoustic oscillations limit the acceptable operating range and increase the risk of fatigue-induced mechanical failure in gas turbine combustor design [1], [2]. Optimization approaches aimed at identifying optimal combinations of geometrical and operational parameters can help mitigate these instabilities by reducing the likelihood of thermoacoustic instability. Traditionally, adjoint-based techniques—mathematical tools derived from the system's governing equations—have been widely employed to evaluate the effects of design or operational changes on thermoacoustic eigenvalues and overall system stability.

Recently, data-driven optimization methods have gained traction, as they require no prior knowledge of the system's underlying physics. These black-box approaches assess performance improvements and iteratively adjust parameters based on empirical data. A key element in understanding thermoacoustic behavior is the flame transfer function (FTF), which describes the relationship between fluctuations in the flame's heat release rate and the acoustic inlet velocity[3-6]. The FTF characterizes the dynamic response of the flame to acoustic excitation, dependent on the amplitude of velocity fluctuations, $|u'/\bar{u}|$, and the excitation frequency, f. Mathematically, the FTF is expressed as:

$$FTF(f, |u'/\bar{u}|) = \frac{Q'/\bar{Q}}{U'/\bar{U}} \tag{1}$$

where U' represents fluctuations in acoustic velocity, $\bar{U}$ denotes the mean flow velocity, Q' indicates variations in the flame's heat release rate, and $\bar{Q}$ is the mean heat release rate. The FTF consists of two key components: gain and phase. The gain reflects the amplitude ratio between heat release rate fluctuations and acoustic velocity variations, while the phase represents the time delay or phase shift between the acoustic disturbances and the resulting heat release oscillations. In practice, fluctuations in heat release are often inferred from optical measurements, such as chemiluminescence, due to their non-intrusive nature [7]. This allows for an accurate assessment of the flame's response to acoustic excitation without direct interference.

$$Q'/\bar{Q} = I'/\bar{I} \tag{2}$$

This substitution can infer heat release kinetics from optical data [8]. Accurately estimating the FTF is crucial for understanding and controlling thermoacoustic instabilities in combustion systems. While conventional linear and empirical models provide valuable insights, they often fail to capture the complex interactions and nonlinear behavior observed in real-world systems. Data-driven and hybrid models significantly improve system safety and FTF prediction accuracy. Recent advances in machine learning (ML) provide a promising alternative, with the potential to enhance real-time control of combustion systems, leading to improvements in both performance and safety.

ML models can detect instabilities early and provide real-time corrective actions, thereby improving the safety and reliability of combustion systems. In gas turbines and rocket engines, ML-based control systems enable dynamic adjustments based on FTF predictions, reducing system wear and mitigating the risk of catastrophic failures. The growing capabilities of ML in predicting flame behavior across various combustion scenarios have been demonstrated in recent studies. For

instance, Wu et al. [9] employed Transformer encoders and Long Short-Term Memory (LSTM) networks in combination with neural networks and frequency-sweeping techniques to model nonlinear flame behavior. Similarly, Shen and Morgans [10] showed that a multi-layer perceptron model with physics-informed preprocessing outperforms earlier algorithms in predicting hydrogen-enriched flame responses to acoustic excitation. Neural networks have also been used to simulate the linear and nonlinear response of turbulent flames to broadband acoustic forcing [11].

In recent work by Akhtardanesh et al. [12], machine learning techniques were applied to determine optimal acoustic power levels for flame extinction. Acoustic power at the point of extinction is a critical metric in understanding combustion dynamics. Four key parameters—frequency, equivalence ratio, wall diameter ratio, and Reynolds number—were used as inputs for a supervised ML model, specifically Support Vector Regression (SVR). The model was trained to predict the acoustic power required for flame extinction in methane and propane fuels. Evaluations using the R-squared metric demonstrated the model's accuracy and robust performance across different conditions.

This research focuses on experimentally predicting the Flame Transfer Function (FTF) of a methane-air flame under a range of acoustic disturbances. The flame was acoustically excited using an experimental test rig, and OH* chemiluminescence was used to capture the heat release rate. High-speed imaging of the flame was processed to ensure the repeatability of key parameters, including flame area, thickness, position, and heat release. The deep learning model developed in this study accurately predicted the nonlinear FTF and was validated against both simple and complex signals. By providing practical experimental validation across varying frequencies and pressure amplitudes, this approach offers valuable insights into the dynamic behavior of combustion systems, expanding the predictive capability of flame response models.

2. Experimental procedure

2.1. Setup and diagnostics

Fig. 1 illustrates the experimental setup of the counterflow burner used in the Advanced Combustion Laboratory, Department of Aerospace Engineering, Sharif University of Technology [13-17]. The test rig consists of two identical sections (top and bottom), each equipped with a 0.125 mm mesh grid to ensure a uniform exit velocity profile over a 31.5 cm pipe. Additional components include a converging nozzle, a honeycomb-structured plenum, a flash-back arrestor, and a loudspeaker. Loudspeakers (Vibe Black Air 12), with a frequency range of 20–1200 Hz, are positioned at the base of the plenums to generate modulated acoustic waves. The plenums have an inner diameter of 30.5 cm, while the concentrically aligned exit nozzles are 2.54 cm in diameter, with a spacing (L) of 2.0 cm and a geometric tolerance of ±0.05 mm. A nitrogen coflow (purity 99.99%) is introduced in the lower section of the burner at a minimum flow rate of 20 L/min to protect the flame from environmental disturbances and guide the hot reaction products. This prevents interaction between the nozzle streams and ambient air during acoustic excitations.

The acoustic waves are generated using a signal generator software, amplified through Hertz HCP 1DK amplifiers, and their amplitudes are measured with a Sound Pressure Level (SPL) meter (B&K 2250) with ±1.5 dB accuracy over the 3–20,000 Hz range. The acoustic characteristics of the feeding blocks were determined for 1 to 50 Watts of input power over 10–200 Hz at the nozzle exit. The Helmholtz resonance frequency of the plenum chamber, calculated using standard

relations, was approximately 45 Hz, and measurements confirmed that the strongest waves occur between 40 and 50 Hz. Acoustic frequencies between 20 and 350 Hz were used to excite the flame, with lower frequencies excluded due to speaker limitations and higher frequencies omitted as the flame showed insensitivity.

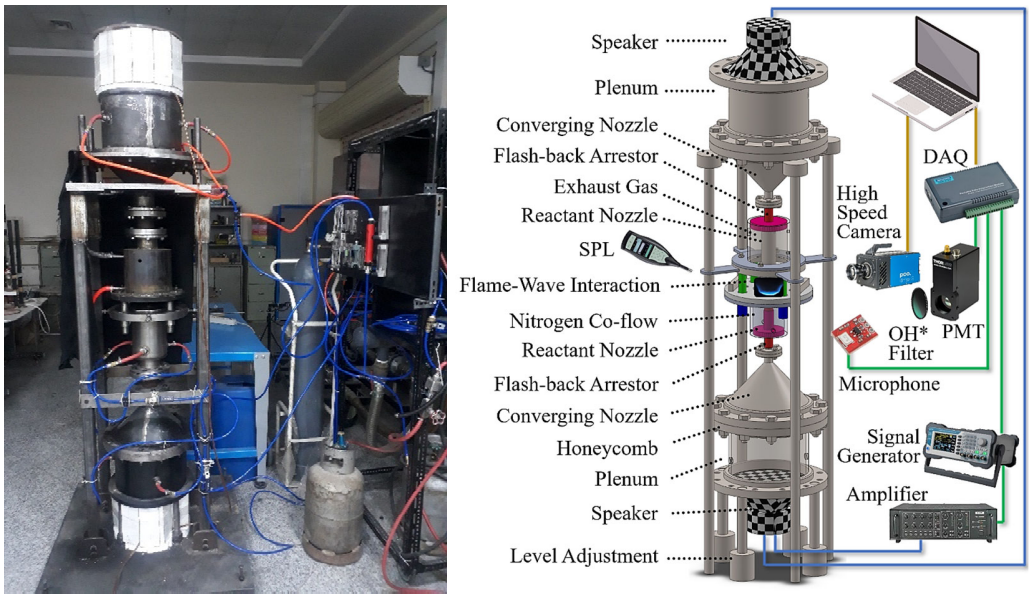

Fig. 1. Schematic representation of the combustion instability laboratory, experimental equipment (right), and the physical setup (left).

The chemiluminescence intensity of OH* and CH* radicals was a reliable indicator of the heat release rate [18]. Measurements were conducted using a photomultiplier tube (Thorlabs, PMM01) equipped with OH* and CH* filters (ASAHI Spectra, XHQA310, and XBPA430, centered at 310 and 430 nm, respectively, with 10 nm bandwidths and efficiencies of 60% and 85%). Non-intrusive CH* chemiluminescence was captured using a high-speed CMOS camera (1920 fps, 1280×720 pixels) with a 430 ± 10 nm bandpass filter. A microphone at the nozzle exit recorded phase lag between acoustic pressure signals and photomultiplier outputs. Additionally, digital image processing in MATLAB was employed to extract CH* intensity distributions from RGB high-speed images using methods validated in previous studies.

2.2. Flow condition

A 99.99% pure nitrogen (N_2) jacket was used to prevent interaction between the ambient air and the nozzle streams during the experiments, maintaining a minimum flow rate of 20 L/min to ensure the flame reaction zone remained undisturbed during acoustic excitations. In all experiments, 15 L/min of air from the top nozzle, along with 15 L/min of air and 2.25 L/min of methane from the bottom nozzle in the premixed regime, entered the flame reaction zone. This setup ensured that observed variations were solely due to flame-acoustic interactions, with no influence from hydrodynamics or reaction kinetics.

The effects of steady harmonic acoustic oscillations with varying amplitudes on the structure of partially premixed counterflow flames were examined within the frequency range of 20 to 350 Hz. Lower frequencies were excluded due to acoustic exciter limitations, while higher frequencies

were omitted as the flame showed insensitivity to them. The wavelength of acoustic waves (17.3 to 1 meter) was significantly larger than the flame thickness, suggesting planar wave interactions within the burner nozzle.

2.3. Acoustic driver evaluation

Acoustic drivers, like any dynamic system, exhibit a response function. Experimental tests were conducted to evaluate the driver's ability to generate waves with the desired amplitude and phase. Pressure amplitudes of 3, 5, and 7 Pa were generated across the 20 to 350 Hz frequency range by adjusting the driver's voltage and input current. The results, shown in Fig. 2, include wave amplitudes at the nozzle outlet measured using an SPL meter and the phase difference between the signal generator and acoustic driver determined via a DAQ system with a 3500 Hz sampling rate.

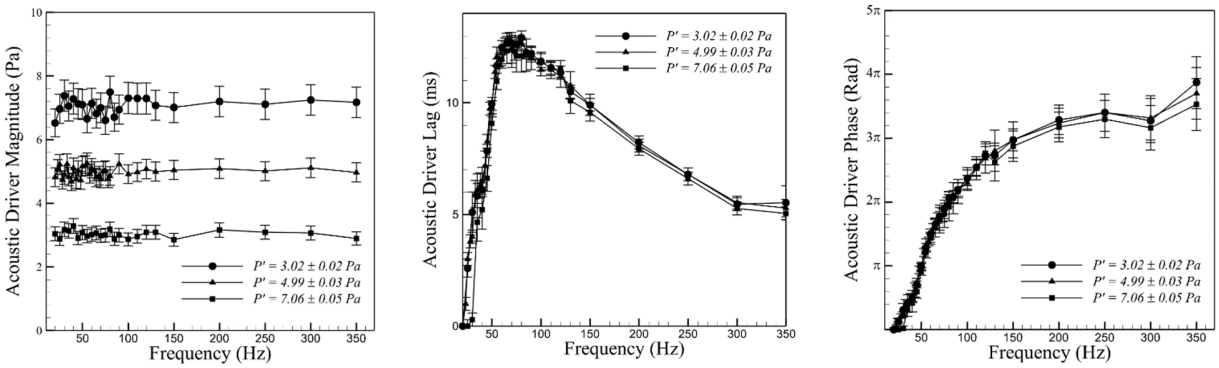

Fig. 2. Measured magnitude (left), time lag (middle) and phase difference (right) between acoustic driver and signal generator

At frequencies below 30 Hz, the time delay between the signal generator and the acoustic driver was negligible, with a maximum time delay of 12.8 ms observed at 65 Hz. As the frequency increased to 350 Hz, this time delay reduced to 5 ms. Importantly, the time delay in acoustic wave production was independent of wave amplitude. A phase difference curve was plotted by comparing the time delay with the wave period, showing an ascending trend with increasing frequency. However, the phase difference was not affected by wave amplitude. At frequencies above 50 Hz, the phase difference error was on the order of the data acquisition error (1/3500 = 0.29 ms), whereas at frequencies below 50 Hz, uncertainty in the phase difference increased.

3. Processing of the experimental data

It is essential to define the flame's instantaneous quantities with precision mathematically to analyze the physical phenomena governing the problem. As illustrated in Fig. 3, the instantaneous flame thickness is taken as the distance between the highest and lowest pixels of the smoothed image at the flame's center. The flame surface area is calculated by counting the illuminated pixels (with a minimum light intensity of 20 units) and multiplying by the pixel's longitudinal and transverse dimensions. The radiation intensity is calculated by integrating the brightness intensity of all pixels in the filtered image. This radiation intensity corresponds to the emission at a wavelength of 430 nanometres, representing the instantaneous radiation intensity of the excited methylidyne radical and the instantaneous heat release rate in the flame. The flame displacement

is calculated along the flame's central symmetry line using equation (3) since the flame edges are constantly changing shape. In this correlation, y_i is the pixel distance from the centre of the lower nozzle, I_i is the pixel radiation intensity at a wavelength of 430 nanometres and Y_{CoHR} is the center of the flame radiation area at that moment. The entire process was implemented and executed within an image processing code in MATLAB. The uncertainties in the measurements were minimal, with relative errors of ± 2.5% for CH* intensity $\bar{I}_{CH}$, ± 1.8% for flame thickness $\bar{t}$, ± 4.1% for flame area $\bar{A}$, and ± 0.7% for flame displacement $\bar{Y}_{CoHR}$. A detailed discussion of uncertainty sources and error analysis is provided in [16].

$$Y_{CoHR}=\left(\sum y_i I_i\right)/\left(\sum I_i\right) \tag{2}$$

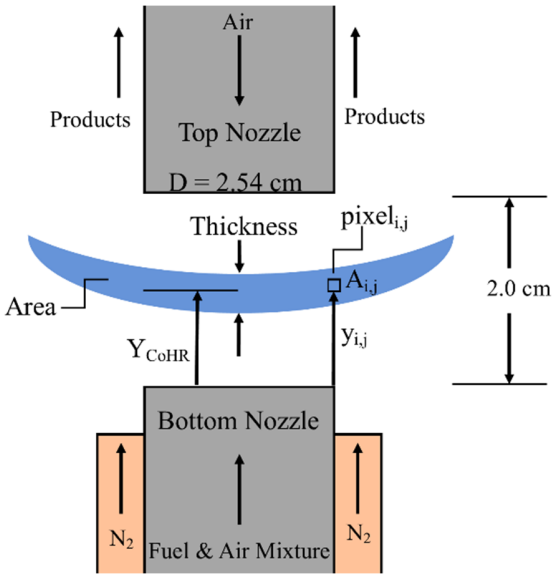

Fig. 3. Illustration of area, thickness, displacement of the center of heat release of counterflow flame

To evaluate the repeatability of the experimental results, the counterflow flame was tested three separate times at a fixed frequency of 40 Hz and an excitation amplitude of 5 Pascal. Fig. 4 presents high-speed images of the flame structure across eight frames for six consecutive cycles, along with the cycle-averaged image. The Abel inverse transformation method [19] was applied to derive cross-sectional views of the flame along the central plane. Fig. 5 provides quantitative results from the high-speed image analysis in Fig. 4, covering four key parameters: nondimensionalized fluctuations of instantaneous CH* intensity ($Q'/\bar{Q} \approx CH'/\overline{CH}$), flame area, flame thickness, and displacement of the heat release center. The results demonstrate a calculation error of less than 0.4% for the mean flame surface position and the radiation intensity of CH* radical (430 nm) across all three tests. Additionally, an analysis of 100 excitation cycles revealed that the error in calculating the amplitude of fluctuations in both the displacement of the radiation center and the intensity of the excited methylidyne radical was less than 1.6%.

The findings from previous studies on premixed flames have established a direct relationship between flame surface area and heat release rate, expressed as $Q \propto A$ [20]. Under linear velocity fluctuation conditions, where $\frac{U'}{\bar{U}} \ll 1$ and the oscillations remain within the linear regime, it has

been shown that $Q'/\bar{Q} \approx A'/\bar{A}$ [21]. Furthermore, chemiluminescence measurements have confirmed a linear correlation between the radiation intensity and the flame surface area, $\bar{I}_{CH} \propto \bar{A}$ [22]. These prior findings are consistent with the results illustrated in Fig. 5, reinforcing the validity of the experimental observations.

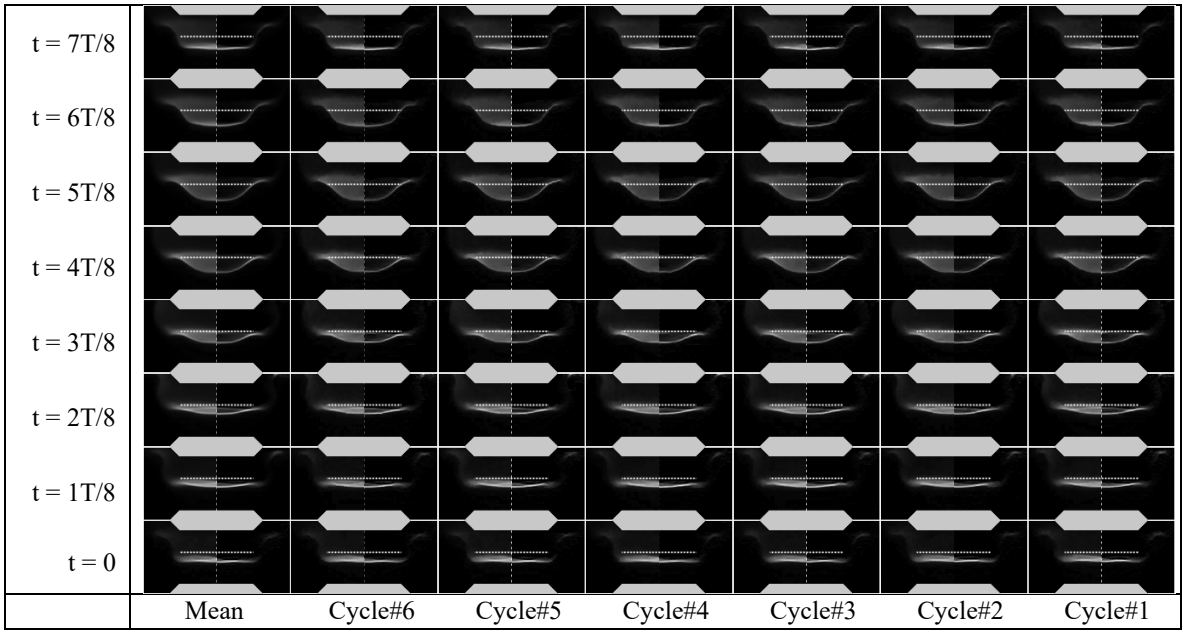

Fig. 4. Instantaneous CH* chemiluminescence images (left) and their corresponding Abel transformations (right) during acoustic excitation at f = 40 Hz and P' = 5 Pa, shown for six consecutive cycles and the cycle-averaged result. The horizontal dashed line represents the stationary stagnation plane.

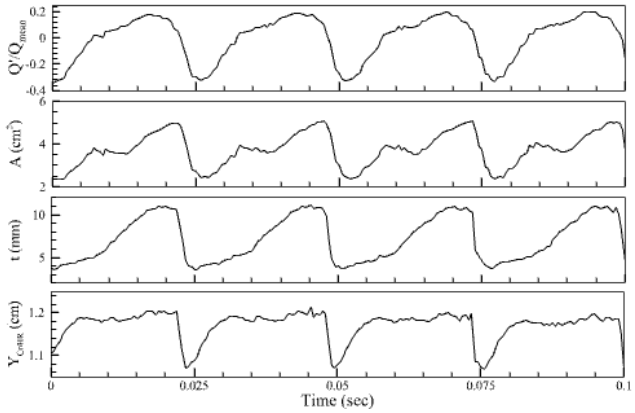

Fig. 5. Instantaneous Y_{CoHR}, thickness, area, and the heat release ratio of the excited flame (f = 40 Hz and P'= 5 Pa) captured using high-speed imaging.

The repeatability of the flame-acoustic interaction over time ensures that a dynamic system can be developed with a well-designed deep learning model to predict the flame's response to acoustic excitation accurately. By training the model across a wide range of acoustic pressure amplitudes and frequencies, capturing the complex, nonlinear interactions between the flame and the acoustic field would be possible. This approach can enhance real-time control and prediction of combustion dynamics, leading to more reliable and efficient combustion systems.

4. Deep learning model

In this paper, a hybrid deep learning architecture is introduced that integrates Convolutional Neural Networks (CNNs) [23], [24] with Transformer mechanisms [25] to process the time series sequential data effectively. The training and testing datasets were derived from two distinct experimental runs, ensuring no overlap to prevent data leakage. The input features consist of acoustic pressure, which characterizes the temporal and spectral dynamics of the acoustic excitation. The target output is the heat release response, quantifying the system's reaction to acoustic perturbations.

The input features and the target output were normalized to ensure consistency and remove scale dependency. The scaler was first fit to the training data to compute the mean and standard deviation, and the same parameters were applied to the test set. This normalization process ensures uniformity, accelerates model convergence, and stabilizes training. Given the time series nature of the data, a sequence length of 30 time steps was selected to account for temporal dependencies in the inputs. The target output was aligned with the input sequences to enable one-step-ahead predictions of the heat release response. This structured preprocessing pipeline ensures that the model leverages temporal patterns in the acoustic pressure input to effectively predict the heat release response.

The proposed deep learning framework comprises two distinct parts, as shown in Fig. 6. The CNN component employs a hierarchical structure, incrementally increasing the filter count from 16 to 128 across four layers. Each layer captures progressively abstract features of the input, leveraging techniques such as batch normalization for improved convergence and average pooling to downsample spatial dimensions, thereby enhancing computational efficiency. A shape-matching procedure ensures alignment to harmonize the dimensions of feature maps produced by the CNN layers, enabling their concatenation into a unified feature representation. This consolidated feature map is then passed through a dense layer that reduces its dimensionality, preparing it for further processing by the Transformer module.

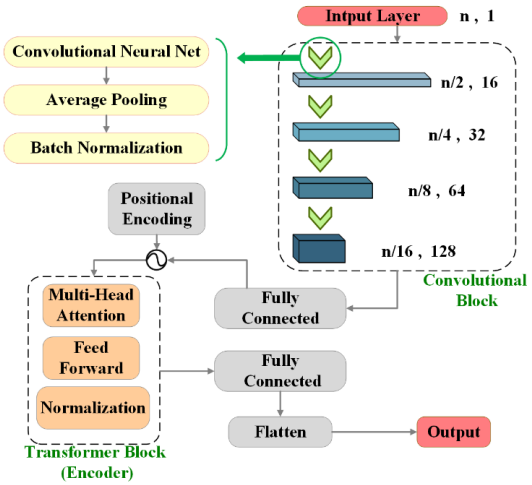

Fig. 6. The framework of the proposed deep learning model for FTF prediction

The Transformer block is a crucial architecture component that captures local and global temporal dependencies in sequential data. The block employs a multi-head self-attention mechanism at its core. It is implemented through the Multi-Head Attention layer with four parallel attention heads

and a feature dimension of 32 per head. This self-attention mechanism uses the same tensor for query, key, and value inputs, enabling the model to learn intricate relationships between all positions within the sequence. The outputs from the attention heads are concatenated and linearly transformed, allowing the model to focus on multiple aspects of the input simultaneously. A dropout layer with a 10% rate is applied to mitigate overfitting. Additionally, layer normalization with a small epsilon ($\epsilon=1\times10^{-6}$) ensures numerical stability by normalizing the outputs across features, facilitating a smoother learning process. Together, these components enable the Transformer block to model complex dependencies across sequential data with enhanced robustness and generalization capabilities.

In the final stage, dense layers refine the processed features before the output layer predicts a scalar value. This strategic integration of CNN-driven hierarchical feature extraction and Transformer-based dependency modeling offers a powerful framework for sequential data analysis, balancing model complexity with predictive performance. Table 1 provides a summary of key components of the model architecture.

Table. 1. The Details of the Neural Network Model

Layers	Number of Filters/ Units	Kernel Size	Activation Function	Pooling Size
CNN - Layer 1	16	3	tanh	2
CNN - Layer 2	32	3	tanh	2
CNN - Layer 3	64	3	tanh	2
CNN - Layer 4	128	3	tanh	2
Fully Connected (Dense Layer)	32	-	ReLu	-
Output Layer	1	-	Linear	-

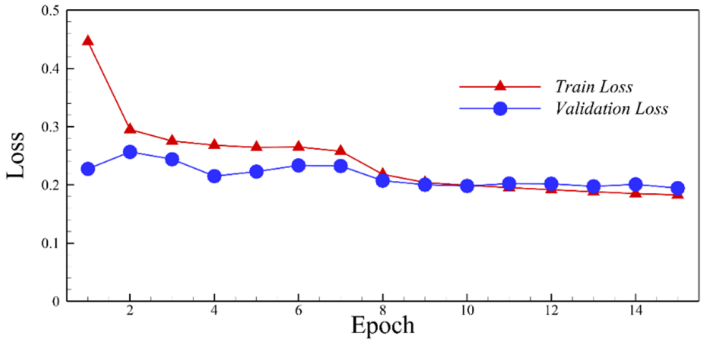

Fig. 7. Train Loss and Validation Loss curves of the model.

The dataset was divided into training (80%) and testing (20%) subsets, with 10% of the training data allocated for validation. The Adam optimizer was employed for its adaptive learning capabilities, with the loss function defined as Mean Squared Error (MSE) and Mean Absolute Error (MAE) used as the evaluation metric. The training was conducted using a batch size of 16 over 50 epochs.

Several callbacks were employed to enhance training stability:

- Early stopping monitored validation loss with patience of five epochs to prevent overfitting.
- A learning rate scheduler reduced the learning rate by 20% if validation loss plateaued for three consecutive epochs, with a minimum learning rate of 1×10^{-5}.

The training process tracked the loss (MSE) across the training and validation datasets. Fig. 7 depicts the loss curves, illustrating the model's performance over time.

4.1. Data acquisition

Acoustic oscillations' frequency and amplitude have the biggest effects on the FTF. The essential frequency response for partially premixed counterflow flames is below 100 Hz. Saitoh and Otsuka [26] observed that the oscillation amplitude approached zero at 100 Hz for ethylene counterflow flames and diminished further as the frequency increased. Similarly, according to Brown and Pitz [27], methane-air non-premixed counterflow flames did not exhibit appreciable structural changes over 200 Hz. Consequently, as illustrated in Fig. 8, data for model training were selected from six frequency or amplitude ranges. The red line shows the heat release reaction as determined by OH* chemiluminescence, while the blue line reflects the input pressure signal to the acoustic driver. The acoustic wave amplitude was progressively increased until the flame reached the acoustic extinction point in tests conducted at constant frequencies (regions a, b, and c). Acoustic extinction prevented the higher amplitudes from being included [28],[17],[28-30]. The amplitude increased by 1 Pascal every two seconds until extinction in region "A" where the frequency was maintained at 30 Hz.

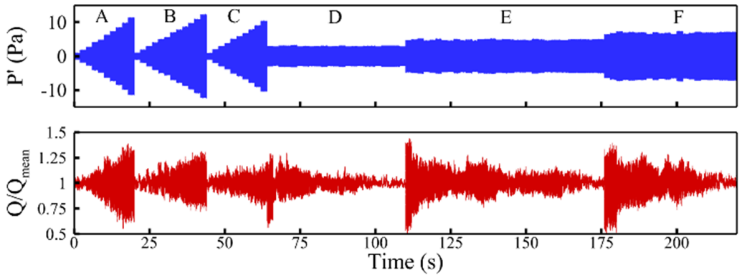

Fig. 8. Training data from experimental measurements for deep learning: Input acoustic pressure (top) and the corresponding heat release response (bottom).

The same amplitude increments were applied at a frequency of 60 Hz in region "B" and at 90 Hz in region "C". In the tests conducted in regions D, E, and F, the frequency changed between 20 and 350 Hz while the amplitude of the acoustic wave remained constant. Each test took two seconds to train the model. The amplitude was fixed at 3 Pascal in region D and set to 5 and 7 Pascal in regions E and F, respectively. Data from the input and output signals were gathered at a sampling rate of 3500 Hz for every test.

5. Results and discussion

The model's performance was evaluated using test data, including acoustic excitations not used during training. The model accurately predicted the chemiluminescence signal, closely matching experimental measurements and demonstrating a robust understanding of the flame response function. Initially, a sinusoidal signal with a frequency of 30 Hz and a constant pressure amplitude of 5 Pascals was input into the trained model. The predicted results were compared against

experimental data, as shown in Fig. 9 (top). The model successfully captured the mean value, amplitude, and phase differences of the output signals with high precision. While the predicted output followed a sinusoidal waveform, minor deviations in amplitude and phase at 30 Hz were observed, likely due to experimental uncertainties and the nonlinear interactions between the acoustic field and the combustion process.

In the second stage, triangular waveforms with the same amplitude and frequency were used to assess the model's performance further. As depicted in Fig. 9 (middle), the model produced a smoothed triangular signal, a result of the non-differentiable points in the input signal. This deviation was influenced by two factors: the non-ideal behavior of the acoustic exciter, which could not perfectly replicate the triangular shape, and the dynamic response of the sensors, which affected the signal's fidelity. Despite these factors, the transformer model displayed satisfactory predictive accuracy.

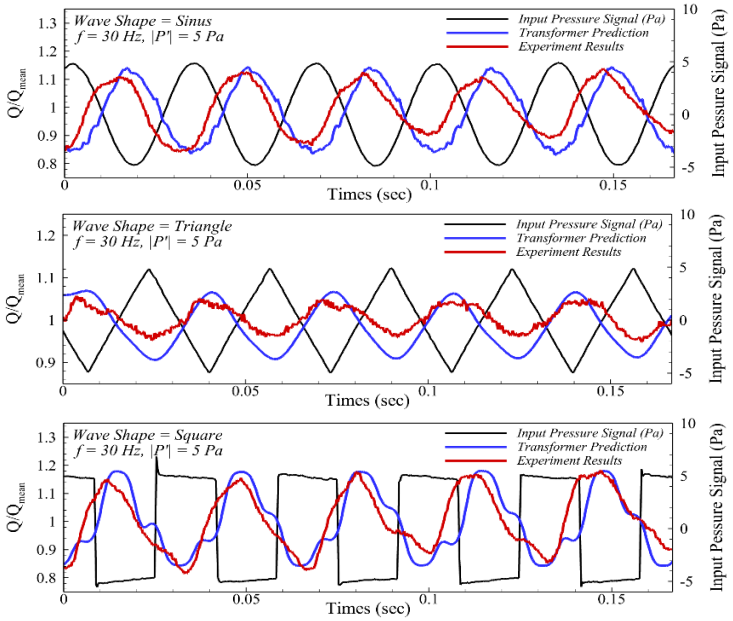

Fig. 9. Validation of the square (bottom), the triangle (middle) and the sinus (top) signals at a constant f = 30 Hz and the pressure amplitude of 5 Pa. The black thin line: is the pressure input signal, the blue thick line: is the results predicted by CNNs + Transformer, and the red thick line: is the experimental results

The third stage of testing involved square waveforms at a constant amplitude of 5 Pascals and a frequency of 30 Hz. Fig. 9 (bottom) illustrates that the experimental flame response and the model's predictions resulted in a distorted square wave. This distortion stemmed from nonlinearities in the flame's dynamic response, along with inherent limitations of the sensors and acoustic actuators. Despite these challenges, the model's predictions are closely aligned with experimental data. The peaks and overshoots in the acoustic pressure input, particularly at signal extremums, influenced corresponding extremums in the predicted output. The model accurately predicted the phase delay and mean heat release rate, although variations in the amplitude of heat release rate oscillations were noted across different input signal frequencies.

Thus far, the analyses have focused on the flame response under constant pressure or frequency conditions. The dynamic response of the flame was examined to evaluate the model's performance across the entire range of frequencies and pressure amplitudes. The flame response function was

extracted at three excitation pressure levels—3, 5, and 7 Pascals—over the frequency range of 20 to 350 Hz. Fig. 10 compares the magnitude (top) and phase (bottom) of the flame's dynamic response obtained experimentally with the results from the deep learning model.

At low frequencies (f = 20 Hz), the counterflow flame exhibits oscillations in the heat release rate that are of the same order of magnitude (O(1)) as the input acoustic velocity amplitude, a characteristic also observed in simple flames, such as conical flames [31]. The flame response function behaves like a low-pass filter, allowing low-frequency oscillations to pass while attenuating higher frequencies, showing a dynamic behavior comparable to Bunsen flames [5]. As the frequency increases (f > 80 Hz), the acoustic field loses its influence on the flame area, and the fluctuations in heat release rate diminish to less than 10% of the mean values, leading to a downward trend in the gain.

The phase difference between the fluctuations in heat release rate and the velocity exhibits linear behavior in the frequency range of 20 to 350 Hz. However, the slope of this linearity shifts near 50 Hz. Below 50 Hz, the slope of the phase difference is $d\varphi/df = 0.033\pi$, whereas at frequencies above 100 Hz, it increases to $d\varphi/df = 0.053\pi$. In modeling the flame response function of simple flames, such as conical flames, it is generally assumed that disturbances travel with the mean flow velocity, introducing a delay of $\varphi = 2\pi f\tau$ [32]. According to this model, the time delay between the fluctuations in heat release rate and the acoustic velocity is approximately 16.7 ms for excitation frequencies below 50 Hz and 26.6 ms for frequencies above 100 Hz.

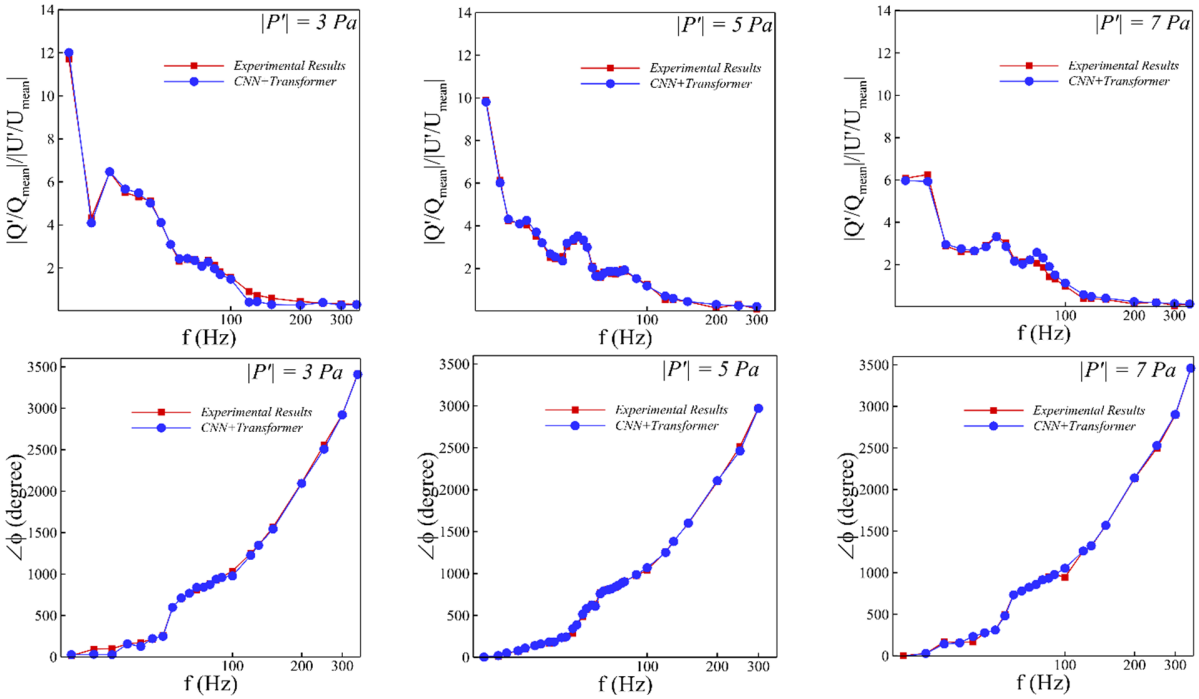

Fig. 10. Gain (top) and phase (bottom) of the flame response function for the counterflow flame under varying excitation pressure amplitudes of 3, 5, and 7 Pa. Red lines represent experimental data, while blue circles indicate predictions from the deep learning model.

The experimental results and the deep learning model exhibited consistent phase and gain across all tested frequencies and pressure amplitudes of the acoustic waves. Within the frequency range of 20 to 150 Hz, the flame response magnitude showed excellent agreement between the two

methods, validating the model's ability to capture the flame's dynamic behavior. At frequencies exceeding 150 Hz, the experimental flame response and the deep learning model prediction converged toward zero. This behavior is notable, as uncertainties in experimental data at higher frequencies, driven by increased sensitivity to environmental disturbances, challenge the model's ability to capture the flame dynamics accurately. The training dataset for the deep learning model was optimized by reducing the sampling size at higher frequencies to address this limitation. This adjustment effectively minimized the influence of external disturbances, enhancing the model's predictive accuracy in this frequency range. The improved dataset refinement highlights the importance of adapting data preprocessing techniques to achieve robust predictions under varying experimental conditions.

6. Conclusion

This study presents a deep learning framework for predicting the dynamic response of a partially premixed methane-air counterflow flame under acoustic excitation. The flame's heat release rate was measured using OH* chemiluminescence across a frequency range of 20 to 350 Hz and pressure amplitudes extending to the extinction point. A hybrid model was trained on experimental data, combining Convolutional Neural Networks (CNNs) for feature extraction and a Transformer Encoder for behavior forecasting. The repeatability of the flame structure was rigorously validated through high-speed imaging and image processing, confirming consistent flame characteristics, such as area, thickness, and heat release displacement, across multiple tests.

The model demonstrated excellent agreement with experimental data, accurately predicting phase and gain across all frequencies and pressure amplitudes. It replicated experimental amplitude, phase, and mean heat release rates with high fidelity for sinusoidal signals. Minor amplitude discrepancies were observed for more complex triangular and square signals, primarily due to actuator and sensor limitations. Both experimental and model results exhibited low-pass filter behavior, with significant attenuation of heat release fluctuations above 80 Hz and near-zero responses beyond 150 Hz due to experimental constraints. Optimizing the training dataset at higher frequencies further improved the model's ability to capture high-frequency dynamics.

Overall, the deep learning approach used in this study offers a reliable and practical tool for predicting flame response under various acoustic conditions. It is a valuable asset in addressing combustion instabilities in engineering applications. Future advancements in data acquisition and sampling techniques could further enhance model accuracy, particularly at higher frequencies, thereby broadening its applicability in real-world systems.

Author declarations

Conflict of interest

The authors have no relevant financial or non-financial interests to disclose.

Credit authorship contribution statement

Mohammad Ali Akhtardanesh: Conceptualization, Data curation, Investigation, Methodology, Software, Simulation, Validation, Experimental setup, signal processing, Visualization, Writing –

original draft, Writing – review & editing. **Ensieh Alipour:** Formal Analysis, Investigation, Methodology, Software, Visualization, ML implementation, Writing – original draft, review & editing. **Mohammad Farshchi:** Conceptualization, Funding acquisition, Experimental setup, Data curation, Methodology, Investigation, Project administration, Supervision, Writing – review & editing.

Acknowledgments

The authors would like to express their deepest gratitude to Mr. Meysam Khadem Alrezaeian for his valuable contributions to the design, construction, and commissioning of the burner. Special thanks are also extended to Dr. Fathollah Ommi, a faculty member of Tarbiat Modarres University, for his support in providing the equipment for the experimental setup used in the acoustic excitation of counterflow flames.

References

[1] T. Poinsot, Prediction and control of combustion instabilities in real engines, Proceedings of the Combustion Institute, Vol. 36, Iss. 1, 1-28 (2017).

[2] S. Candel, Combustion dynamics and control: Progress and challenges, Proceedings of the combustion institute, Vol. 29, Iss. 1, 1-28 (2002).

[3] A.-L. Birbaud, D. Durox, S. Ducruix, S. Candel, Dynamics of confined premixed flames submitted to upstream acoustic modulations, Proceedings of the Combustion Institute, Vol. 31, Iss. 1, 1257-1265 (2007).

[4] T. Schuller, D. Durox, S. Candel, Self-induced combustion oscillations of laminar premixed flames stabilized on annular burners, Combustion and flame, Vol. 135, Iss. 4, 525-537 (2003).

[5] D. Durox, T. Schuller, N. Noiray, S. Candel, Experimental analysis of nonlinear flame transfer functions for different flame geometries, Proceedings of the Combustion Institute, Vol. 32, Iss. 1, 1391-1398 (2009).

[6] D. Durox, T. Schuller, S. Candel, Combustion dynamics of inverted conical flames, Proceedings of the combustion Institute, Vol. 30, Iss. 2, 1717-1724 (2005).

[7] M.A. Akhtardanesh, M. Farshchi, M. Ranjbar Najafi, M.J. Hosseinkhani, Analysis of CH and OH chemiluminescence in the dynamic study of a partially
premixed counterflow flame, in: Fuel and combustion Tehran: Iranian Society of Fuel and Combustion,, 2024

[8] F.G. Schiavone, A. Aniello, E. Riber, T. Schuller, D. Laera, On the adequacy of OH* as heat release marker for hydrogen–air flames, Proceedings of the Combustion Institute, Vol. 40, Iss. 1-4, 105248 (2024).

[9] J. Wu, J. Nan, L. Yang, J. Li, Reconstruction of the flame nonlinear response using deep learning algorithms, Physics of Fluids, Vol. 35, Iss. 1, (2023).

[10] Y. Shen, A.S. Morgans, Predicting the effect of hydrogen enrichment on the flame describing function using machine learning, International Journal of Hydrogen Energy, Vol. 79, 267-276 (2024).

[11] C.E. Üstün, M.R. Herfatmanesh, A. Valera-Medina, A. Paykani, Applying machine learning techniques to predict laminar burning velocity for ammonia/hydrogen/air mixtures, Energy and AI, Vol. 13, 100270 (2023).

[12] M.A. Akhtardanesh, E. Alipour, S.M.B. Malaek, Application of machine learning to bring efficiency to costly experiments: case of flame-extinction, Fuel and Combustion, Vol. 17, Iss. 2, 20-36 (2024).

[13] M. Akhtardanesh, M.K. Alrezaeian, M. Farshchi, Interaction of acoustic waves with a laminar counterflow flame, in: 9th National Conference of Acoustical Society of Iran, 2023

[14] M.A. Akhtardanesh, M.K. Alrezaeian, M. Farshchi, A Comparison between methane and propane counterflow flame acoustic excitation in the partially premixed regime, in: 20th Fluid Dynamics Conference, Tehran: the physics society of iran, 2023

[15] M.A. Akhtardanesh, M.J. Hosseinkhani, M. Farshchi, The effect of hydrogen addition on the acoustic response of a partially premixed counterflow flame, Fuel and combustion, Vol. 16, Iss. 4, 43-60 (2024).

[16] M.A. Akhtardanesh, M. Khademorezaeian, M. Farshchi, Interaction of acoustic waves with a laminar counterflow flame, Journal of Acoustical Engineering Society of Iran, Vol. 11, Iss. 2, 55-65 (in persian) (2024).

[17] M.A. Akhtardanesh, M.J. Hosseinkhani, M. Farshchi, Acoustic extintion of partially premixed counterflow flame, The Journal of Engine Research, Vol. 70, Iss. 3, 39-552 (2023).

[18] Y. Hardalupas, M. Orain, Local measurements of the time-dependent heat release rate and equivalence ratio using chemiluminescent emission from a flame, Combustion and Flame, Vol. 139, Iss. 3, 188-207 (2004).

[19] Y. Cho, S.-J. Na, Application of abel inversion in real-time calculations for circularly and elliptically symmetric radiation sources, Measurement science and technology, Vol. 16, Iss. 3, 878-884 (2005).

[20] V. Kornilov, K. Schreel, L. De Goey, Experimental assessment of the acoustic response of laminar premixed Bunsen flames, Proceedings of the Combustion Institute, Vol. 31, Iss. 1, 1239-1246 (2007).

[21] S. Schlimpert, M. Meinke, W. Schröder, Nonlinear analysis of an acoustically excited laminar premixed flame, Combustion and Flame, Vol. 163, 337-357 (2016).

[22] K.M. Kopp-Vaughan, S.G. Tuttle, M.W. Renfro, G.B. King, Heat release and flame structure measurements of self-excited acoustically-driven premixed methane flames, Combustion and Flame, Vol. 156, Iss. 10, 1971-1982 (2009).

[23] Y. LeCun, L. Bottou, Y. Bengio, P. Haffner, Gradient-based learning applied to document recognition, Proceedings of the IEEE, Vol. 86, Iss. 11, 2278-2324 (1998).

[24] J. Heaton, I. Goodfellow, Y. Bengio, A. Courville, Deep learning, Genetic Programming and Evolvable Machines, Vol. 19, Iss. 1-2, 305–307 (2018).

[25] A. Vaswani, N. Shazeer, N. Parmar, J. Uszkoreit, L. Jones, A.N. Gomez, Ł. Kaiser, I. Polosukhin, Attention is all you need, Proceedings of the 31st International Conference on Neural Information Processing Systems, 6000-6010 (2017).

[26] T. Saitoh, Y. Otsuka, Unsteady behavior of diffusion flames and premixed flames for counter flow geometry, Combustion Science and Technology, Vol. 12, Iss. 4-6, 135-146 (1976).

[27] T. Brown, R. Pitz, Experimental investigation of counterflow diffusion flames with oscillatory stretch, 34th Aerospace Sciences Meeting and Exhibit, 1996, pp. 214.

[28] M. Akhtardanesh, M.K. Alrezaeian, M. Hosseinkhani, M. Farshchi, An experimental study on bunsen flame acoustic extinction, in: The 21st International Conference of Iranian Aeropace Association, Tehran, 2022

[29] M.A. Akhtardanesh, M.J. Hosseinkhani, M. Farshchi, Acoustic Extintion of Partially Premixed Counterflow flame, in: 20th Fluid Dynamics Conference, Tehran: the physics society of iran, 2023

[30] E. Alipour, M.A. Akhtardanesh, S.M.B. Malaek, Application of machine learning to bring efficiency to costly experiments ; case of flame-extinction, in: Tenth Fuel and combustion conference of Iran, Tehran, 2024

[31] W. Polifke, C. Lawn, On the low-frequency limit of flame transfer functions, Combustion and flame, Vol. 151, Iss. 3, 437-451 (2007).

[32] Y. Matsui, An experimental study on pyro-acoustic amplification of premixed laminar flames, Combustion and Flame, Vol. 43, 199-209 (1981).